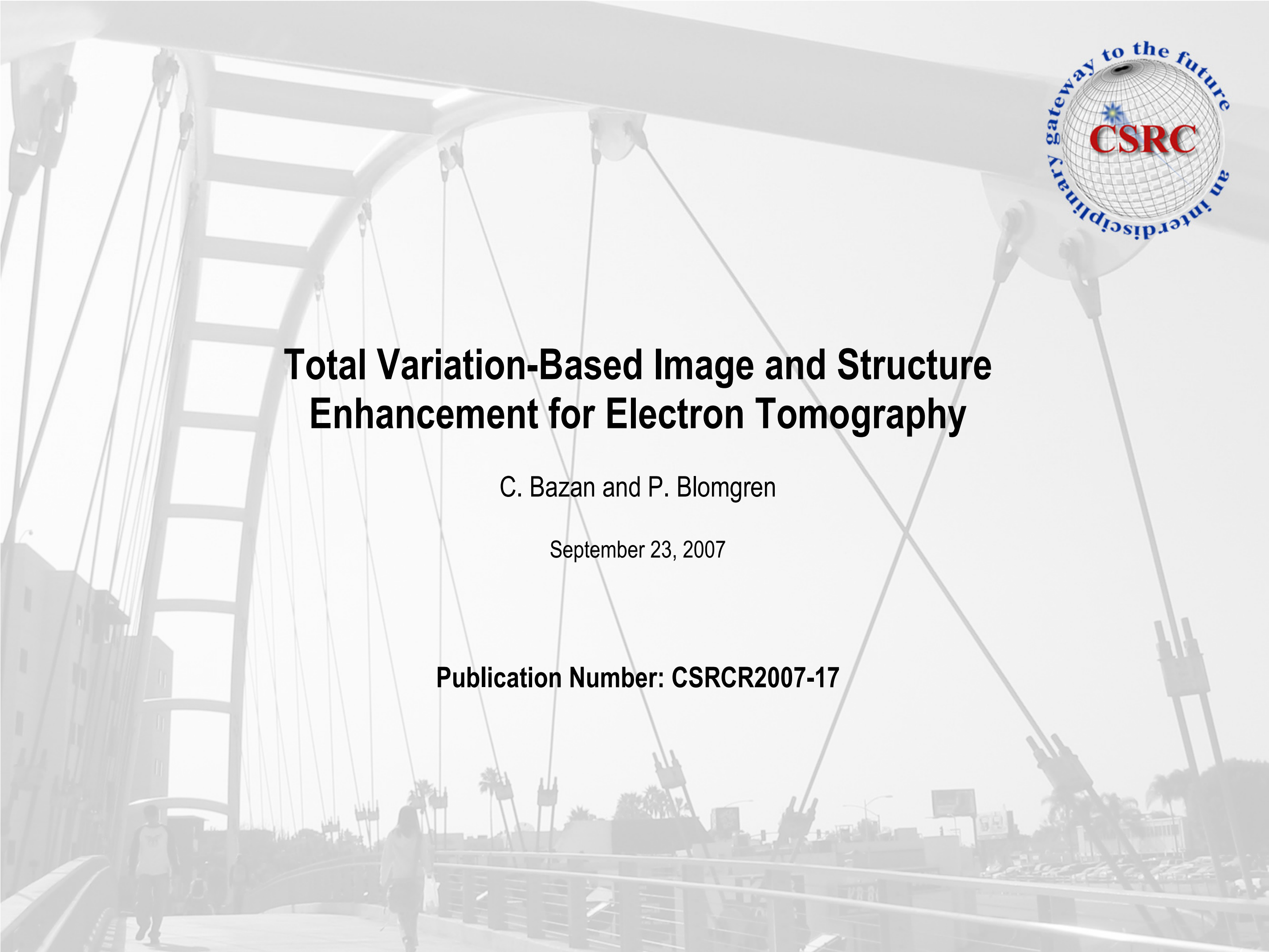

Total Variation-Based Image and Structure Enhancement for Electron Tomography

C. Bazan and P. Blomgren

September 23, 2007

Publication Number: CSRCR2007-17

COMPUTATIONAL SCIENCE & ENGINEERING

SAN DIEGO STATE UNIVERSITY

Computational Science Research Center
College of Sciences
5500 Campanile Drive
San Diego, CA 92182-1245
(619) 594-3430

Total Variation–Based Image and Structure Enhancement for Electron Tomography

Carlos Bazan* and Peter Blomgren†

September 23, 2007

Abstract

We introduce total variation–based methods for the reduction of noise and the enhancement of mitochondrion structure for electron tomography. We perform a comparative study between two total variation-based image noise removal techniques, applied to electron microscopic imaging of a mitochondrion. Our tests show that both methods perform extremely well at removing the multiplicative noise present in this type of imagery. The methods facilitate the segmentation that will allow extraction and rendering of a 3D structural model of the mitochondrion. The structural information contributes to the better interpretation, measurement, and understanding of the intricate mitochondrial architecture and its relation to functionality.

1 Introduction

To date, it is firmly established that mitochondrial function plays an important role in the regulation of apoptosis (programmed cell death) [24]. There is also evidence that defects in function may be related to many of the most common diseases of aging, such as Alzheimer dementia, Parkinson's disease, type II diabetes mellitus, stroke, atherosclerotic heart disease and cancer [43]. This belief is founded in the observation that mitochondrial function experiences measurable disturbance and observable morphological changes under these circumstances [43, 16]. Electron tomography (ET) has allowed significant advances in the understanding of mitochondrial structures. This imaging technique currently provides the highest 3D resolution of the internal structure of mitochondria in thick sections. Despite the recent advances in imaging hardware and specimen fixation techniques, it has been argued in the structural biology community [16] that the image processing methodologies in the 3D ET field are not yet sufficiently developed, so as to correctly extract features and understand spatial relationships in mitochondrial structures. There is a strong need for a set of image processing methodologies that will facilitate efficient reconstruction and analysis of the data obtained via ET.

*Computational Sciece Research Center, San Diego State University, 5500 Campanile Dr, San Diego, CA 92182-1245, carlos.bazan@sdsu.edu

†Department of Mathematics & Statistics, Dynamical Systems Group & Computational Sciece Research Center, San Diego State University, 5500 Campanile Dr, San Diego, CA 92182-7720, blomgren@terminus.sdsu.edu

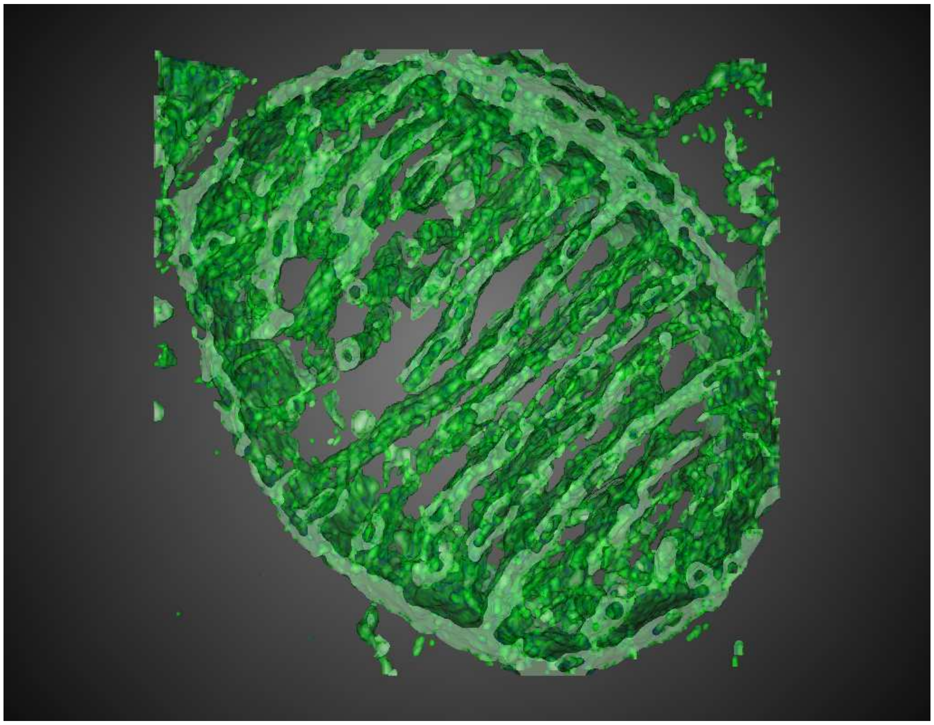

Figure 1: Cross-section rendering of a mitochondrion 3D tomogram after applying the homomorphic TV-based image and structure enhancement algorithm for ET.

In this paper we use total variation (TV) based methods for the reduction of noise and the enhancement of mitochondrion structure for ET. These methods are used prior to applying image segmentation techniques that facilitate the 3D rendering and subsequence analysis of the mitochondrion structure (see Fig. 1). We design an algorithm based on the classic TV-based method by Rudin, Osher and Fatemi [47] within a homomorphic system, and compare it to the TV-based image restoration technique by Rudin, Lions and Osher [46] for reducing the multiplicative noise present in electron microscopy (EM) imagery. In a homomorphic system, the natural logarithm is used to transform the multiplicative nature of the degradation into an additive one and then, the resulting degraded image is processed by using a filter to reduce the additive white noise. An exponential function is then applied to the output of the filter. The TV constrained optimization approach involves the variation (oscillations) of the image within its domain, subject to constraints related to the statistics of the noise. The procedure leads to a nonlinear partial differential equation on a manifold determined by the constraints which is solved by a time-evolution scheme.

There is a number of reasons for preferring TV-based models over their counterparts. TV-based algorithms are relatively simple to implement and result in minimal ringing (non-oscillatory) while recovering sharp edges (noninvasive) [46]. In other words, the bounded variation (BV) norm allows piecewise smooth functions with jumps and is the proper space for the analysis and recovery of discontinuous functions. Linear methods, such as those based on the minimization of the gradient's L^2-norm or some higher derivatives as in [30, 53, 54] cannot satisfy the axioms of morphology [6]. It has been also stated [50] that the use of linear filters in the homomorphic system would not be effective when the additive noise deviates from the Gaussian distribution. In such a case, the use of nonlinear filters in the homomorphic system have proven to be more effective. Furthermore, empirical evidence suggests that the human vision favors the L^1-norm [12]. Therefore, the TV-based formulation is the proper approach to restoring piecewise continuous functions from noisy and blurry signals.

The paper is organized as follows: In Section 2, we discuss the statistical properties of images corrupted by multiplicative noise, as well as the statistical properties of the corresponding log-transformed images. In Section 3, we present the two TV-based formulations, namely the classic Rudin-Osher-Fatemi method [47] for additive noise applied within a homomorphic system, and the Rudin-Lions-Osher model [46] for multiplicative noise. In Section 4, we evaluate the performance of the two TV-based noise removal techniques applied to a 2D electron tomogram slice. Finally, in Section 5, we conclude with a summary and discussion of our findings, and outline the steps necessary for performing a fully 3D image reconstruction of electron tomograms.

2 Modeling the Noise in Electron Microscopy

2.1 Nature of the noise

Images generated by coherent imaging systems are always degraded by speckle noise [19, 50, 59]. Coherent imaging systems are very common in many applications such as synthetic aperture radar (SAR), ultrasound, laser imaging, and EM. In EM, speckle is generated by the random elastic (and inelastic) scattering of electron beams as they pass through the specimen [37]. The noise appears as dark and bright granulations and it limits the ability of both manual and automatic interpretation and understanding of the registered image.

Speckle is usually considered a type of multiplicative noise [19, 50]. Most modern electron microscopes are equipped with charge-coupled device (CCD)[1] cameras for capturing the images. In a CCD camera, images are generally corrupted by both additive and multiplicative noise [58]. In the more general CCD camera noise model [27], the following contributions are present: dark current noise, shot noise, readout noise, and quantization noise. However, it has been shown [58] that the amount of multiplicative noise exceeds the

[1] There are also available the high-end electron multiplying charge-coupled device (EMCCD) cameras and intensified charge-coupled device (ICCD) cameras.

amount of additive noise at intensities greater than 10 to 30% of the intensity range. Therefore, for most practical applications we can disregard the additive portion of the noise, including the quantization noise.

2.2 Noise Statistics

Speckle can be either partially or fully developed depending on the scatter number density [1]. Fully developed speckle has the characteristics of random multiplicative noise [23, 57, 59]. Most researchers agree that the noise in a single image corrupted by speckle follows a negative exponential distribution [22, 23, 28, 55, 57]. When speckle is reduced by image integration, such as in multi-look averaging (SAR) and image back-projection (used in EM), the resultant speckle is characterized as following either a Gamma distribution [3, 13, 15, 22, 28, 55, 57] or a Log-normal distribution [4, 19, 50][2]. In the case of multi-look images, it has been stated [19] that using either the gamma distribution or the Log-normal distribution to model the speckle does not result in a significant difference in the filter performance.

To take advantage of available and well established denoising methods, it is often necessary to apply a logarithmic transformation to convert the multiplicative model into an additive model. However, care must be taken when applying approaches based on additive noise models directly to a log-transformed signal. The logarithmic transformation is a nonlinear operation that can completely change the statistics of the image [59]. This issue has been addressed by a few authors [29, 32, 59] and the probability density function, mean value, and variance which characterizes the log-transformed speckle have been devised [59]. (It has been also found that applying the logarithmic transformation to the signal perturbed by fully developed speckle is very close to Gaussian distribution [1, 13, 26].) It has been also conjectured that the Gaussian distribution approximation can be considered in the case of partially developed speckle [1, 13]. This implies, that after an image integration, the Log-normal distribution could be safely used to approximate the intensity distribution of the speckle [50].

2.3 Adopted Noise Model

In a digital signal, the noise degradation of a multiplicative nature can be interpreted as each sample of the true signal being multiplied by a random noise element. A 2D tomographic slice can be represented as

$$f(x, y) = g(x, y)\, m(x, y), \tag{1}$$

[2] As the number of images integrated tends to infinity, the speckle intensity tends to follow a Gaussian distribution [7, 23].

where $f(x,y)$ is the observed degraded image, $g(x,y)$ is the true image, and $m(x,y)$ is the multiplicative noise with unit-mean following a Gamma probability distribution. Applying the natural logarithmic transform (homomorphic system) of the observed corrupted image we can write

$$\begin{aligned} \ln f(x,y) &= \ln g(x,y) + \ln m(x,y) \\ &= \tilde{g}(x,y) + \tilde{m}(x,y), \end{aligned} \tag{2}$$

which can be written as

$$u_0(x,y) = u(x,y) + \eta(x,y). \tag{3}$$

In (3), $\eta(x,y)$ is a random zero-mean stationary white noise process [52] and $u(x,y) = \ln g(x,y) + \mu_{\tilde{m}}$, where $\mu_{\tilde{m}}$ is the mean of $\tilde{m}$. The variance and mean of $\tilde{m}$ has been derived in [59] for an integer number of looks L:

$$\mu_{\tilde{m}} = -\gamma_{EM} - \ln(L) + \sum_{k=1}^{L-1} \frac{1}{k}, \tag{4}$$

$$\sigma_{\tilde{m}}^2 = \frac{\pi^2}{6} - \sum_{k=1}^{L-1} \frac{1}{k^2}. \tag{5}$$

In (4), $\gamma_{EM} = 0.577215664901...$ is the Euler-Mascheroni constant.

3 Noise Reduction Techniques

Most of the multiplicative noise reduction techniques employ some variation of Oppenhein's homomorphic systems [42]. Oppenhein introduced the idea of a canonical form of a system comprising a point operation to convert the signal and noise combination to an additive one. Then, he applied a linear system to suppress the now additive noise, and finally an inverse point operation to return the processed signal and noise to the original intensity domain. In the present, a number of methods (using this approach) exist to address the problem of speckle noise including median filtering [11, 21], temporal averaging [9, 19], geometry-based filtering [10], nonlinear multiscale filtering [60], adaptive speckle reduction [8, 14, 17, 33, 34, 36, 38, 39, 40], homomorphic Wiener filtering [5, 19, 20, 31], wavelet [18, 19, 25, 28, 35, 41, 49] and curvelet [48, 49, 51, 56].

We will use a similar approach as above for our "homomorphic TV image denoising" technique. The problem we are trying to solve is (1) where the electron tomogram has been corrupted by multiplicative noise. We will start by considering a 2D slice (see Fig. 2) that we want to restore prior to applying the segmentation technique that will allow better classification and interpretation. For the homomorphic TV method, we recast (3) as

$$u_0 = u + \eta. \tag{6}$$

Our constrained minimization problem is

$$\underset{u\in BV(\Omega)}{\text{minimize}} \int_\Omega \sqrt{u_x^2 + u_y^2}, \tag{7}$$

where Ω represents the domain of the image, subject to the following constraints involving the statistics of the signal and the noise

$$\int_\Omega u \; dxdy = \int_\Omega u_0 dxdy, \tag{8}$$

$$\int_\Omega (u - u_0)^2 \, dxdy = |\Omega| \, \sigma_\eta^2. \tag{9}$$

Constraint (8) suggests that the mean of the noise is zero, thus the mean of the intensity values of the image remains constant, while constraint (9) implies that the standard deviation of the noise, σ_η, is known *a priori*. Using Lagrange multipliers to minimize this constrained optimization problem leads to the Euler-Lagrange equations

$$0 = \frac{\partial}{\partial x}\left(\frac{u_x}{\sqrt{u_x^2 + u_y^2}}\right) + \frac{\partial}{\partial y}\left(\frac{u_y}{\sqrt{u_x^2 + u_y^2}}\right) - \lambda\,(u - u_0) \qquad \text{in } \Omega, \tag{10}$$

$$\frac{\partial u}{\partial \mathbf{n}} = 0 \qquad \text{on } \partial\Omega. \tag{11}$$

The solution procedure proposed in [47] uses a parabolic equation with time as an evolution (scale) parameter, or equivalently, the gradient descent method. This is

$$\frac{\partial u}{\partial t} = \frac{\partial}{\partial x}\left(\frac{u_x}{\sqrt{u_x^2 + u_y^2}}\right) + \frac{\partial}{\partial y}\left(\frac{u_y}{\sqrt{u_x^2 + u_y^2}}\right) - \lambda\,(u - u_0)\,, \tag{12}$$

in Ω, for $t > 0$, with homogeneous Neumann boundary condition $\partial_{\mathbf{n}} u = 0$ on $\partial\Omega$, and $u\,(0, x, y) = u_0$ is the observed image used as initial condition. For the parameter λ the authors suggested a dynamic value $\lambda\,(t)$ estimated by Rosen's gradient-projection method [44, 45], which as $t \to \infty$ converges to

$$-\frac{1}{2\,|\Omega|\,\sigma_\eta^2} \int_\Omega \left(\sqrt{u_x^2 + u_y^2} - \frac{(u_0)_x\, u_x}{\sqrt{u_x^2 + u_y^2}} - \frac{(u_0)_y\, u_y}{\sqrt{u_x^2 + u_y^2}}\right) dxdy. \tag{13}$$

For our second TV-based implementation [46], we solve (1) in its original form

$$f = gm. \tag{14}$$

In doing so, we again minimize the TV of the image

$$\underset{g \in BV(\Omega)}{\text{minimize}} \int_{\Omega} \sqrt{g_x^2 + g_y^2}, \tag{15}$$

subject to the following constraints involving the statistics of the noise

$$\int m = 1, \quad \forall g \qquad \text{or} \qquad \int_{\Omega} m = |\Omega|, \tag{16}$$

$$\int (m-1)^2 = \sigma_m^2, \quad \forall g \qquad \text{or} \qquad \int_{\Omega} (m-1)^2 = |\Omega| \, \sigma_m^2. \tag{17}$$

Constraint (16) is necessary to account for the case of a noise–free image, while constraint (17) is a direct consequence of (16) and implies that the standard deviation of the noise, σ_m, is also known *a priori*.

Thus, the constrained optimization (15) is subject to the following constraints

$$\int \frac{f}{g} = 1, \tag{18}$$

$$\frac{1}{2} \int \left(\frac{f}{g} - 1 \right)^2 = \frac{1}{2} \int \left(\left(\frac{f}{g} \right)^2 - 1 \right) = \frac{\sigma_m^2}{2}. \tag{19}$$

Using Lagrange multipliers leads to

$$\frac{\partial g}{\partial t} = \frac{\partial}{\partial x} \left(\frac{g_x}{\sqrt{g_x^2 + g_y^2}} \right) + \frac{\partial}{\partial y} \left(\frac{g_y}{\sqrt{g_x^2 + g_y^2}} \right) - \lambda_1 \frac{f^2}{g^3} - \lambda_2 \frac{f}{g^2}, \tag{20}$$

in Ω, for $t > 0$, with homogeneous Neumann boundary condition $\partial_{\mathbf{n}} g = 0$ on $\partial\Omega$, and $g(0, x, y) = f$ is the observed image used as initial condition. We now have two Lagrange multipliers λ_1 and λ_2, which can be computed by requiring

$$\frac{\partial}{\partial t} \int \frac{f}{g} = - \int \frac{f}{g^2} \frac{\partial g}{\partial t} = 0, \quad \forall g \qquad \text{or} \qquad \frac{\partial}{\partial t} \int_{\Omega} \frac{f}{g} = \int_{\Omega} \frac{f}{g^2} \frac{\partial g}{\partial t} = 0, \tag{21}$$

$$
\frac{\partial}{\partial t}\int\left(\left(\frac{f}{g}\right)^2-1\right)=-\int\frac{f^2}{g^3}\frac{\partial g}{\partial t}=0,\quad\forall g
$$
$$
\text{or}\qquad\frac{\partial}{\partial t}\int_\Omega\left(\left(\frac{f}{g}\right)^2-1\right)=\int_\Omega\frac{f^2}{g^3}\frac{\partial g}{\partial t}=0. \tag{22}
$$

These, together with (20), lead to two algebraic equations for the two unknowns and the resulting Gram determinant is nonzero.

4 Experimental Results

4.1 Homomorphic TV-based Additive Noise Removal

For this case, we implemented a slight variation of (12) [2] with Neumann boundary condition and the observed image as initial condition, using finite element method. The parameter λ was implemented as suggested in (13) and for the standard deviation of the noise, σ_η, we used $\sigma_{\tilde{m}}$ as defined in (5) since $\mathrm{var}(\eta)=\mathrm{var}(\tilde{m}-\mu_{\tilde{m}})=\mathrm{var}(\tilde{m})$, assuming the back-projection was performed using 61 micrographs. We need to correct the output u to account for the applied shift $u=\ln g+\mu_{\tilde{m}}$ where $\mu_{\tilde{m}}$ is given by (4), and then apply the exponential transformation to obtain the final approximation to the true image. Finally, we apply gamma correction to the output above to obtain the final image[3]. The resulting image after applying the described technique is shown in Fig. 3, along with the extraction of the mitochondrion structure obtained by automatic segmentation. The obtained results are extremely encouraging.

4.2 TV-based Multiplicative Noise Removal

In this case we implemented (20) with Neumann boundary condition and the observed image as initial condition, also using finite element method. For the parameters λ_1 and λ_2 we solve the two equations with two unknowns and obtained

$$
\lambda_1(t)=\frac{1}{D(x,y)}\left(\int_\Omega\frac{f^2}{g^4}\int_\Omega\frac{f^2}{g^3}B(x,y)-\int_\Omega\frac{f^3}{g^5}\int_\Omega\frac{f}{g^2}B(x,y)\right), \tag{23}
$$

$$
\lambda_2(t)=\frac{1}{D(x,y)}\left(\int_\Omega\frac{f^4}{g^6}\int_\Omega\frac{f}{g^2}B(x,y)-\int_\Omega\frac{f^3}{g^5}\int_\Omega\frac{f^2}{g^3}B(x,y)\right), \tag{24}
$$

[3] Most CCD cameras use some form of gamma adjustment to map the image into the available quantization range in order to obtain a better looking image [58].

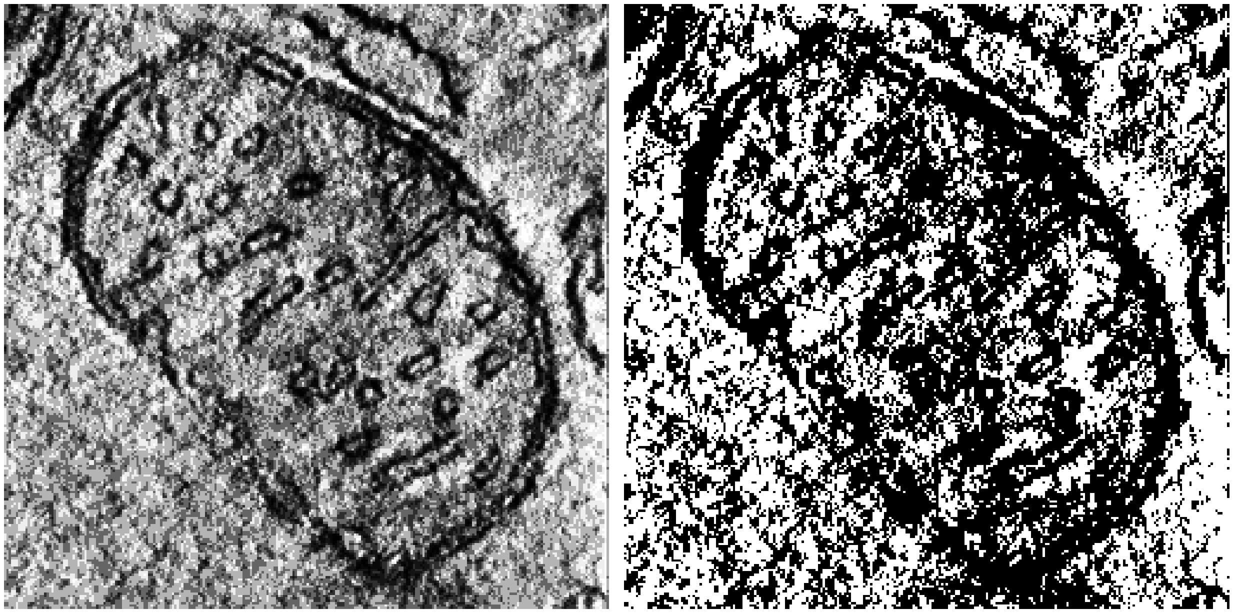

Figure 2: (left) After taking a slice from the 3D electron tomogram of the mitochondrion, through histogram equalization, the intensity range is spread over the entire dynamic range [0, 255]. A linear histogram stretching is used to avoid compromising the statistics of the noise as it would be if gamma correction is employed at this stage. (right) Segmented image using a threshold algorithm before applying the image processing techniques.

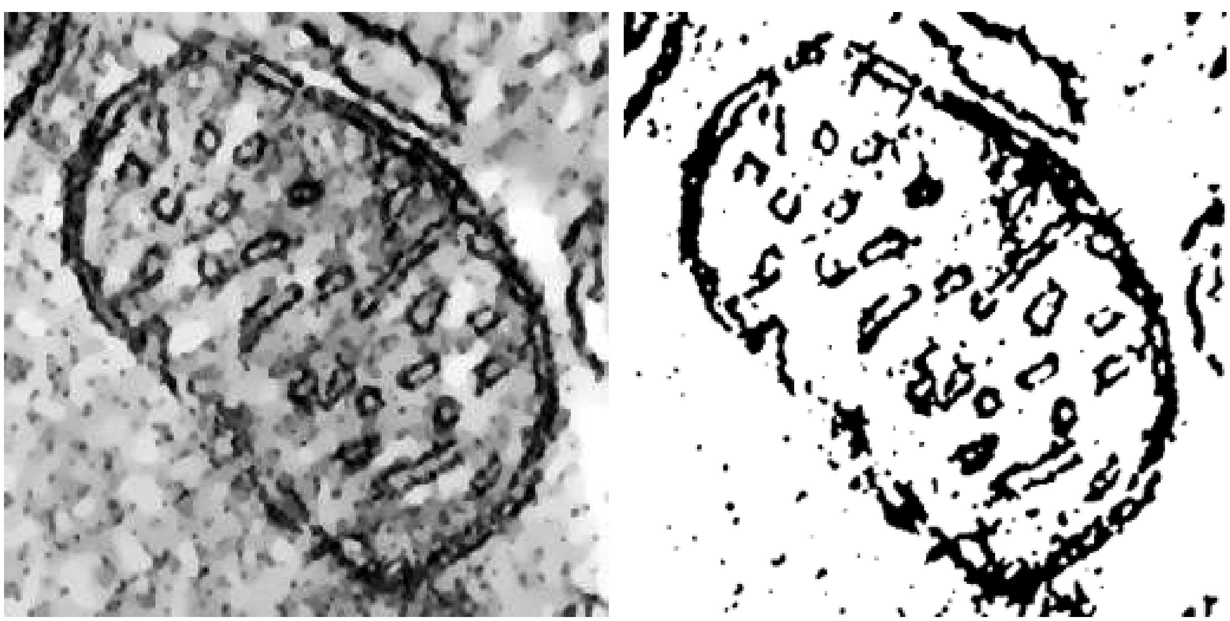

Figure 3: (left) Output image obtained by applying the homomorphic TV–based denoising after gamma correction. We can observe that the image is better suited for automatic segmentation. (right) Segmented image using a threshold algorithm that allows the extraction of the mitochondrion structure.

where

$$D(x,y) = \int_\Omega \frac{f^4}{g^6} \int_\Omega \frac{f^2}{g^4} - \int_\Omega \frac{f^3}{g^5} \int_\Omega \frac{f^3}{g^5}, \tag{25}$$

$$B(x,y) = \frac{g_{xx} + g_{yy}}{\sqrt{g_x^2 + g_y^2}} - \frac{g_x^2 g_{xx} + 2 g_x g_y g_{xy} + g_y^2 g_{yy}}{\left(g_x^2 + g_y^2\right)^{\frac{3}{2}}}. \tag{26}$$

The resulting image after applying the described technique is shown in Fig. 4, along with the extraction of the mitochondrion structure obtained by automatic segmentation. The obtained results are also extremely encouraging.

Figure 4: (left) Output image obtained by applying the TV–based denoising method for multiplicative noise after gamma correction. We can observe that the image is better suited for automatic segmentation. (right) Segmented image that allows the extraction of the mitochondrion structure.

5 Conclusions

We have designed an algorithm based on the classic TV–based model by Rudin, Osher and Fatemi for additive noise removal within a homomorphic system, and compared its performance to that of the TV–based image restoration technique by Rudin, Lions and Osher for reducing multiplicative noise. Both approaches were applied to a stack of 2D images taken from a 3D electron tomogram of a mitochondrion. The image denoising techniques were employed prior to an automatic image segmentation algorithm for the extraction of the mitochondrion's structural details.

Our results show that both methods perform extremely well at removing the multiplicative noise present in this type of image. Once the segmentation has been performed and the structure has been outlined, the 2D images were used to render the 3D structural model of the mitochondrion with relative ease (see Fig. 1). However, the procedure we have employed in this paper has the limitation that the information in the z direction is neglected in favor of simplicity. Our next step will be to carry out a similar approach as the one in this paper, to remove the noise from the 3D tomogram by using a fully 3D approach: 3D histogram stretching, 3D homomorphic TV–based denosing, 3D segmentation, and 3D image rendering. That way, we will obtain an even better approximation to the structure of the mitrochondrion.

6 Acknowledgments

The authors would like to thank Terry Frey and Peter Salamon for providing the electron microscopy images and for their helpful comments on the work. This work has been supported in part by NIH RoadMap Initiative award R90 DK07015.

References

[1] K.Z. Abd-Elmoniem, A.B.M. Youssef, and Y.M. Kadah. Real-time speckle reduction and coherence enhancement in ultrasound imaging via nonlinear anisotropic diffusion. *IEEE Transactions on Biomedical Engineering*, 49(9):997–1014, 2002.

[2] R. Acar and C.R. Vogel. Analysis of total variation penalty methods for ill-posed problems. *Inverse Problems*, 10(6):1217–1229, 1994.

[3] A. Achim, A. Bezerianos, and P. Tsakalides. An alpha-stable based Bayesian algorithm for speckle noise removal in the wavelet domain. In *IEEE - EURASIP Workshop on Nonlinear Signal and Image Processing*, 2001.

[4] A. Achim, P. Tsakalides, and A. Bezerianos. SAR image denoising via bayesian wavelet shrinkage based on heavy-tailed modeling. *IEEE Transactions on Geoscience and Remote Sensing*, 41:1773–1784, 2003.

[5] L. Alparone, F. Boragine, and S. Fini. Parallel architectures for the postprocessing of SAR images. In *SPIE Proceedings*, volume 1360, pages 790–802, 1990.

[6] L. Alvarez, F. Guichard, P.-L. Lions, and J.-M. Morel. Axioms and fundamental equations of image processing. *Archives for Rational Mechanics and Analysis*, 16:199–257, 1993.

[7] H.H. Arsenault and G. April. Properties of speckle integrated with a finite aperture and logarithmically transformed. *Journal of the Optical Society of America*, 66:1160–1163, 1976.

[8] M.R. Azimi-Sadjadi and S. Bannour. Two-dimensional adaptive block Kalman filtering of SAR imagery. *IEEE Transactions on Geoscience and Remote Sensing*, 29:742–753, 1991.

[9] A. Belmonte. Temporal averaging of turbulence-induced uncertainties on coherent power measurements. *Optics Express*, 12(16):3770–3777, 2004.

[10] T.R. Crimmins. Geometric filter for speckle reduction. *Applied Optics*, 24:1438–1443, 1985.

[11] R.N. Czerwinski, D.L. Jones, and W.D. O'Brien. Ultrasound speckle reduction by directional median filtering. In *Proceedings of the EIII International Conference on Image Processing*, volume 1, pages 358–361, 1995.

[12] R. DeVore, B. Jawerth, and B. Lucier. Image compression through wavelet transform coding. *IEEE Transactions on Information Theory*, 38:719–746, 1992.

[13] V. Dutt. *Statistical analysis of ultrasound echo envelope*. PhD thesis, Mayo Graduate School, Rochester, MN, 1995.

[14] S. Foucher, G.B. Bénié, and J.-M. Boucher. Multiscale MAP filtering of SAR images. *IEEE Transactions on Image Processing*, 10(1):49–56, 2001.

[15] S. Foucher, G. Farage, and G. Benie. SAR image filtering based on the stationary contourlet transform. In *Proceedings of IEEE International Conference on Geoscience and Remote Sensing Symposium*, pages 4021–4024, 2006.

[16] T.G. Frey, G.A. Perkins, and M.H. Ellisman. Electron tomography of membrane-bound cellular organelles. *The Annual Review of Biophysics and Biomolecular Structure*, 35:199–224, 2006.

[17] V.S. Frost, J.A. Stiles, K.S. Shanmugan, and J.C. Holtzman. A model for radar images and its application to adaptive digital filtering of multiplicative noise. *IEEE Transactions on Pattern Analysis and Machine Intelligence*, PAMI-4:157–166, 1982.

[18] L. Gagnon, Drissi, and F. Smaili. Speckle noise reduction of airborne SAR images with symmetric daubechies wavelets. In *SPIE Proceedings*, volume 2759, pages 14–24, 1996.

[19] L. Gagnon and A. Jouan. Speckle filtering of SAR images—a comparative study between complex wavelet-based and standard filters. Technical report, Department of R&D, Lockheed Martin, Canada, 1997.

[20] L. Gagnon, H. Oppenheim, and P. Valin. R&D activities in airborne SAR image processing/analysis at Lockheed Martin, Canada. Technical report, Lockheed Martin, Canada, 1998.

[21] N Gallagher, D.W. Sweeney, C.R. Christensen, G.R. Arce, P.K. Murphy, and J.P. Fitch. Speckle noise filtering by use of median filter root signals. *Journal of the Optical Society of America A: Optics, Image Science & Vision*, 72:1743–+, 1982.

[22] J.W. Goodman. *Statistical Properties of Laser Speckle Patterns*. Springer-Verlag, Heidelberg, Germany, 1980.

[23] J.W. Goodman. *Speckle phenomenon in optics: theory and applications*. Roberts and Company, Denver, 2006.

[24] D.R. Green and J.C. Reed. Mitochondria and apoptosis. *Science*, 281(5381):1309–1312, 1998.

[25] H. Guo, J.E. Odegard, M. Lang, R.A. Gopinath, I.W. Selesnick, and C.S. Burrus. Wavelet based speckle reduction with application to SAR based ATD/R. In *IEEE Proceedings of ICIP '94*, pages 75–79, 1994.

[26] N. Gupta, M.N.S. Swamy, and E. Plotkin. Despeckling of medical ultrasound images using data and rate adaptive lossy compression,. *IEEE Transactions on Medical Imaging*, 24(6):743–754, 2005.

[27] G.E. Healey and R. Kondepudy. Radiometric CCD camera calibration and noise estimation. *IEEE Transactions on Pattern Analysis and Machine Intelligence*, 16(3):267–276, 1994.

[28] E. Hervet, R. Fjortoft, P. Marthon, and A. Lopes. Comparison of wavelet-based and statistical speckle filters. In *EUROPTO Conference on SAR Image Analysis, Modeling, and Techniques,*, volume 3497, pages 43–54, 1998.

[29] D.H. Hoekman. Speckle ensemble statistics of logarithmically scaled data. *IEEE Transactions on Geoscience and Remote Sensing*, 29(1):180–182, 1991.

[30] B. Hunt. The application of constraint least-squares estimation to image restoration by digital computer. *IEEE Transactions on Computers*, C-2:805–812, 1973.

[31] A.K. Jain. *Fundamental of Digital Image Processing*. Prentice-Hall, Upper Saddle River, NJ, 1989.

[32] D. Kaplan and Q. Ma. On the statistical characteristics of log-compressed rayleigh signals. In *Proceedings of IEEE Ultrasonics Symposium*, volume 2, pages 961–964, 1993.

[33] D. Kuan, A. Sawchuk, T. Strand, and P. Chavel. Adaptive restoration of images with speckle. *IEEE Transactions on Acoustics, Speech, & Signal Processing*, 35(3):373–383, 1987.

[34] D.T. Kuan, A.A. Sawchuk, T.C. Strand, and P. Chavel. Adaptive noise smoothing filter for images with signal–dependent noise. *IEEE Transactions on Pattern Analysis and Machine Intelligence*, PAMI-7:165–177, 1985.

[35] K. Lebart and J.-M. Boucher. Speckle filtering by wavelet analysis and synthesis. In *SPIE Proceedings*, volume 2825, pages 644–651, 1996.

[36] J.-S. Lee. Digital image enhancement and noise filtering by use of local statistics. *IEEE Transactions on Pattern Analysis and Machine Intelligence*, PAMI-2:165–168, 1980.

[37] B. Lengeler. Coherence. *Applied Physics A*, 87:585–592, 2007.

[38] A. Lopes, E. Nezry, R. Touzi, and H. Laur. Structure detection and statistical adaptive speckle filtering in SAR images. *International Journal of Remote Sensing*, 14(9):17351758, 1993.

[39] K.S. Nathan and J.C. Curlander. Speckle noise reduction of 1-look SAR imagery. In *Proceedings of IGARSS '87 Symposium*, pages 1457–1462, 1987.

[40] C.J. Oddy and A.J. Rye. Segmentation of SAR images using a local similarity rule. *Pattern Recognition Letters*, 1:443–449, 1983.

[41] J.E. Odegard, H. Guo, M. Lang, C.S. Burrus, R.O. Wells Jr., L. M. Novak, and M. Hiett. Wavelet based SAR speckle reduction and image compression. In *SPIE Proceedings*, volume 2487, pages 259–271, 1995.

[42] A. Oppenheim. *Superposition in a Class of Nonlinear Systems*. PhD thesis, Massachusetts Institute of Technology, Cambridge, MA, 1964.

[43] G.A. Perkins and T.G. Frey. Recent structural insight into mitochondria gained by microscopy. *Micron*, 31(1):97–111, 2000.

[44] J.B. Rosen. The gradient projection method for nonlinear programming: Part i, linear constraints. *Journal of Society for Industrial and Applied Mathematics*, 8(1):181–217, 1960.

[45] J.B. Rosen. The gradient projection method for nonlinear programming: Part ii, nonlinear constraints. *Journal of Society for Industrial and Applied Mathematics*, 9(4):514–532, 1961.

[46] L. Rudin, P.-L. Lions, and S. Osher. *Geometric Level Set Methods in Imaging, Vision, and Graphics*, chapter Multiplicative Denoising and Deblurring: Theory and Algorithms. Springer-Verlag, New York, 2003.

[47] L. Rudin, S. Osher, and Fatemi E. Nonlinear total variation based noise removal algorithm. *Physica D*, 60(1/4):259–268, 1992.

[48] B.B. Saevarrson, J.R. Sveinsson, and J.A. Benediktsson. Speckle reduction of SAR images using adaptive curvelet domain. In *Proceedings of IEEE International Geoscience and Remote Sensing Symposium*, volume 6, pages 4083–4085, 2003.

[49] B.B. Saevarrson, J.R. Sveinsson, and J.A. Benediktsson. Combined wavelet and curvelet denoising of SAR images. In 6, editor, *Proceedings of IEEE International Geoscience and Remote Sensing Symposium*, pages 4235–4238, 2004.

[50] D. Sen, M.N.S. Swamy, and M.O. Ahmad. Unbiased homomorphic system and its application in reducing multiplicative noise. *IEE Proceedings Vision, Image, and Signal Processing*, 153(5):521–537, 2006.

[51] J.-L. Starck, E.J. Candès, and D.L. Donoho. The curvelet transform for image denoising. *IEEE Transactions on Image Processing*, 11(6):670–684, 2002.

[52] H.L.V. Trees. *Estimation and modulation theory part I.* John Wiley & Sons, New York, 2001.

[53] S. Twomey. On the numerical solution of fredholm integral equations of the first kind by the inversion of the linear system produced by quadrature. *Journal of the Association for Computing Machinery*, 10:97–101, 1963.

[54] S. Twomey. The application of numerical filtering to the solution of integral equations encountered in indirect sensing measurements. *Journal of Franklin Institute*, 297:95–109, 1965.

[55] F. Ulaby and M.C. Dobson. *Handbook of Radar Scattering Statistics for Terrain.* Artech House, Norwood, MA, 1989.

[56] M.O. Ulfarsson, J.R. Sveinsson, and J.A. Benediktsson. Speckle reduction of SAR images in the curvelet domain. In *Proceedings of IEEE International Geoscience and Remote Sensing Symposium*, volume 1, pages 315–317, 2002.

[57] D.R. Wehner. *High-Resolution Radar.* Artech House, Boston, MA, 2nd edition, 1994.

[58] P.J. Withagen, F.C.A. Groen, and K. Schutte. CCD characterization for a range of color cameras. In *Proceedings of the IEEE Instrumentation and Measurement Technology Conference*, volume 3, pages 2232–2235, 2005.

[59] H. Xie, L.E. Pierce, and F.T. Ulaby. Statistical properties of logarithmically transformed speckle. *IEEE Transactions on Geoscience and Remote Sensing*, 40(3):721–726, 2002.

[60] X. Zong, A.F. Laine, and E.A. Geiser. Speckle reduction and contrast enhancement of echocardiograms via multiscale nonlinear processing. *IEEE Transactions on Medical Imaging*, 17:532–540, 1998.